Vitamin C supramolecular hydrogel for enhanced cancer immunotherapy

Zhang, Han; Liu, Kai; Gong, Yimou; Zhu, Wenjun; Zhu, Jiafei; Pan, Feng; Chao, Yu; Xiao, Zhishen; Liu, Yanbin; Wang, Xianwen

Published in:
Biomaterials

DOI:
10.1016/j.biomaterials.2022.121673

Publication date:
2022

Biomaterials 287 (2022) 121673

Contents lists available at ScienceDirect

Biomaterials

journal homepage: www.elsevier.com/locate/biomaterials

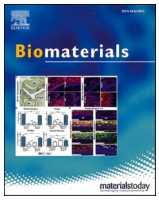

Vitamin C supramolecular hydrogel for enhanced cancer immunotherapy

Han Zhang [a], Kai Liu [b], Yimou Gong [a], Wenjun Zhu [a], Jiafei Zhu [a], Feng Pan [c], Yu Chao [a], Zhishen Xiao [a], Yanbin Liu [a], Xianwen Wang [a], Zhuang Liu [a], Yang Yang [c,**], Qian Chen [a,*]

[a] Institute of Functional Nano & Soft Materials (FUNSOM), Jiangsu Key Laboratory for Carbon-Based Functional Materials & Devices, Soochow University, Suzhou, 215123, China
[b] Centre for Systems Chemistry, Stratingh Institute, University of Groningen, Nijenborgh 4, 9747 AG, Groningen, the Netherlands
[c] Department of Thoracic Surgery, Shanghai Pulmonary Hospital, School of Medicine, Tongji University, Shanghai, 200433, China

ARTICLE INFO

Keywords:
Vitamin C
Self-assembly
Supramolecular hydrogel
Drug delivery
Cancer immunotherapy

ABSTRACT

Vitamin C (VitC) has shown great promise to promote cancer immunotherapy, however, its high hydrophilicity makes it quickly excreted, leading to limited therapeutic efficiency even with frequent high-dose administration. Herein, we provide a pioneering report about the employment of VitC amphiphile self-assembled nanofiber hydrogels for enhanced cancer immunotherapy. Specifically, driven by hydrogen bonding and hydrophobic interactions, the synthesized VitC amphiphile, consisting of a hydrophilic VitC headgroup and a hydrophobic alkyl chain, could self-assemble into an injectable nanofiber hydrogel with self-healing properties. The formed VitC hydrogel not only serves as a reservoir for VitC but also acts as an effective delivery platform for stimulator of interferon genes (STING) agonist-4 (SA). Interestingly, the VitC hydrogel itself exhibits antitumor effects by upregulating genes related to interferon (IFN) signaling, apoptotic signaling and viral recognition and defense. Moreover, the SA-encapsulated VitC hydrogel (SA@VitC hydrogel) synergistically activated the immune system to inhibit the progression of both local and abscopal tumors.

Vitamin C (VitC), a natural bioactive compound with high biosafety and low cost, is emerging as an appealing anticancer candidate [1–3]. Many previous literatures have demonstrated the safety and efficacy of VitC with high dosage after intravenous injection for various cancer treatment [4–6]. Additionally, VitC has also been used in combination with many other therapeutic agents such as DNA methyltransferase inhibitors, chemotherapeutic drugs, and immune checkpoint inhibitors, achieving synergistic therapeutic effects [7–9]. It has been reported that VitC can kill cancer cells by producing hydrogen peroxide via prooxidant effects and disrupting Fe^{2+} metabolism [5,9]. Moreover, VitC usually maintains at high levels in most immune cells and regulates many aspects of immune responses [10,11]. Intracellular VitC can also act as an enzyme cofactor for DNA and histone demethylation reactions to regulate cell phenotype, growth and survival pathways [12–15]. For instance, VitC has been shown to upregulate endogenous retroviruses (ERVs) in lymphoma cells, which can trigger interferon responses by activating the viral defense pathway to activate the immune system to recognize tumor cells [12]. Furthermore, it has also been reported that VitC can promote both the innate and adaptive immune responses by epigenetically modulating T cells [13,14]. However, these unique functions of VitC, such as activating immune cells, only work at very high local concentrations [15,16]. Considering the hydrophilic characteristic of VitC, it usually exhibits quick excretion *in vivo* and leads to limited efficiency in activating immune cells [17,18]. To achieve ideal therapeutic efficiency, VitC at a high dosage is administered intravenously with high frequency, which may cause inconvenience to patients with repeated injection [19]. Moreover, the systemic adverse effects of long-term and repeated injections of VitC are still unclear [20]. Thus, it is of great significance to develop an advanced VitC delivery system to achieve high local concentrations in the long term to effectively promote cancer immunotherapy.

Hydrogels are highly appealing drug delivery systems with high local concentrations, sustained release profiles, long-term retention, and minimal adverse effects [21–24]. For supramolecular hydrogels self-assembled by weak and dynamic noncovalent interactions, their structure and physicochemical properties could be easily and flexibly modulated, permitting effective and safe treatment [25,26]. Typically, a self-assembled supramolecular hydrogel with cross-linked nanofibers

* Corresponding author.
** Corresponding author.
E-mail addresses: timyangsh@tongji.edu.cn (Y. Yang), chenqian@suda.edu.cn (Q. Chen).

https://doi.org/10.1016/j.biomaterials.2022.121673
Received 10 March 2022; Received in revised form 30 June 2022; Accepted 6 July 2022
Available online 8 July 2022

usually exhibits quick gel-sol phase transition and self-healing properties, allowing direct injection into the target sites with minimal invasiveness [27–29]. Moreover, such supramolecular hydrogels could effectively encapsulate bioactive substances with different properties (e.g., size and charge) and efficiently deliver them [30–32]. Recently, designing "self-delivery" supramolecular therapeutic hydrogels, which are able to achieve excellent therapeutic effects and deliver other therapeutics, has attracted wide attention [33,34]. Compared to traditional

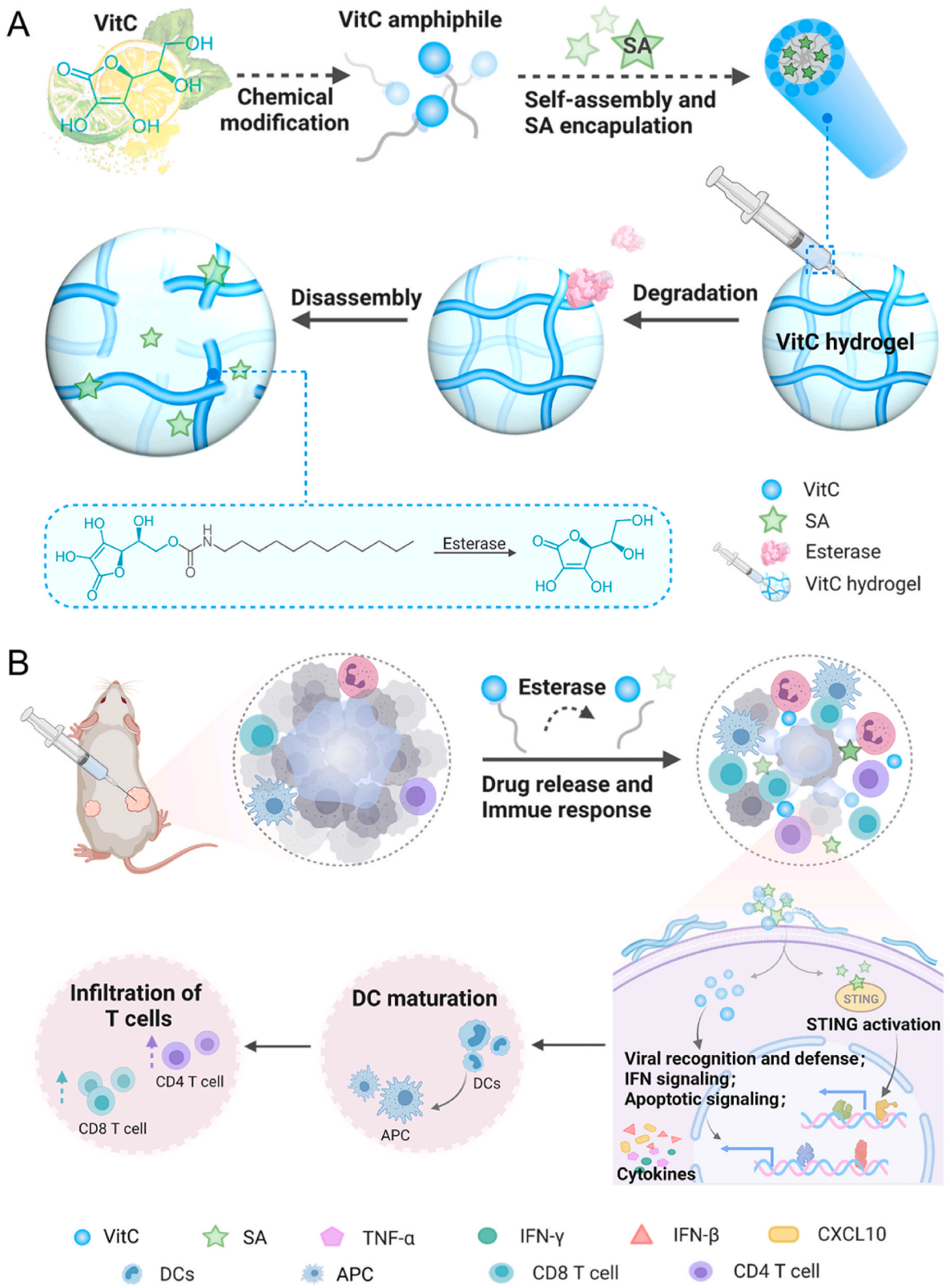

Scheme 1. Schematic illustration of VitC-based nanofiber hydrogels for enhanced cancer immunotherapy. A) The preparation of drug-loaded VitC hydrogel and the release of drugs from the hydrogel. B) Immune responses induced by VitC-based nanofiber hydrogels.

supramolecular hydrogels, self-delivery hydrogels exhibit many other unique advantages, including minimized excipient contents, high drug loading capacity, and synergistic functions with cargo [35–37].

Herein, we provide the first report on the use of a VitC "self-delivery" supramolecular hydrogel to regulate the immune microenvironment, realize efficient delivery of immunologic stimulants, and achieve synergistic immunotherapeutic effects (Scheme 1). First, we synthesized the VitC amphiphile by modifying hydrophilic VitC with a hydrophobic alkyl chain via an ester bond, which is liable for enzymatic digestion *in vivo*. Driven by noncovalent hydrogen-bonding and hydrophobic interactions, VitC amphiphiles could self-assemble into VitC "self-delivery" hydrogels with shear-thinning and self-healing properties. Interestingly, the locally applied VitC hydrogel, acting as VitC depots, could sustainably release VitC to inhibit tumor growth by upregulating genes related to interferon (IFN) signaling, apoptotic signaling and viral recognition and defense. Interferon genes (STING) agonist (SA) effectively activated the STING signaling pathway to vigorously stimulate innate and adaptive immune responses, achieving potent therapeutic results in pre-clinical studies [38–40]. Delivery of SA by VitC hydrogel may achieve synergistic anticancer effects by promoting dendritic cell (DC) maturation and improving the tumor infiltration of natural killer (NK) cells and T cells. Thus, the SA-encapsulated VitC hydrogel (SA@VitC hydrogel) exhibited synergistic antitumor immune responses that significantly impaired the growth of both local and abscopal tumors.

1. Results and discussion

Synthesis and characterization of VitC hydrogel. The gelator, an amphiphile based on VitC, was synthesized as shown in Fig. 1A and Scheme S1 by modifying a dodecyl carbon chain to the hydroxyl at position 6 of VitC. Specifically, we synthesized dibenzyl VitC derivative 3 according to reported procedures [41,42]. Then, dodecyl isocyanate was modified to dibenzyl VitC derivative 3 with carbamate bonds. Finally, the targeted VitC amphiphile was obtained by removing the dibenzyl protection via a hydrogen reduction reaction. The successful

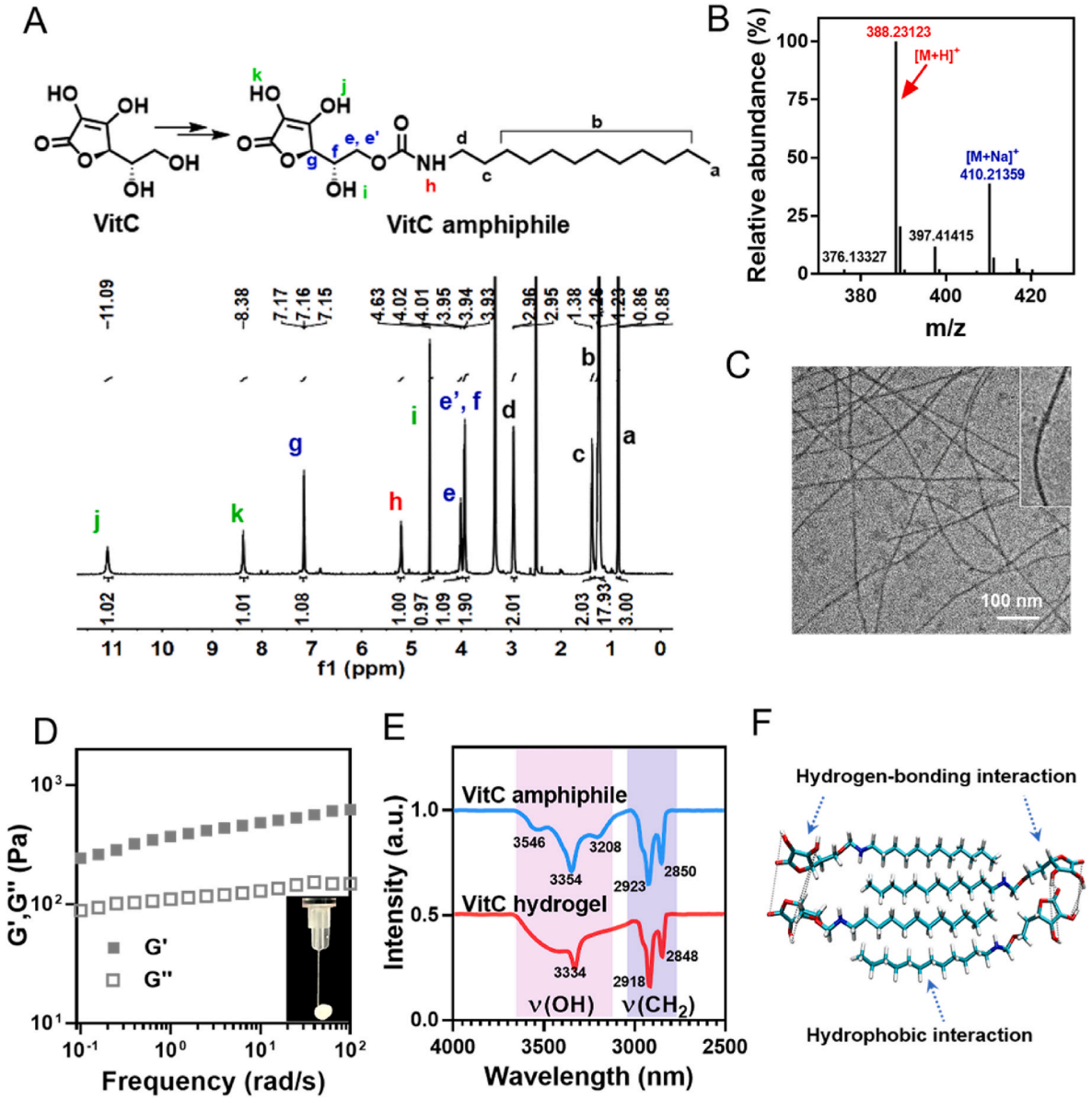

Fig. 1. Preparation and characterization of VitC nanofiber hydrogel. A) ^{1}H NMR and B) HR-MS of the synthesized VitC amphiphile. C) Representative TEM image (insert is the enlarged image) and D) Rheological properties of the VitC hydrogel. E) FTIR spectra of VitC amphiphiles and hydrogel powder. F) Schematic molecular organization pattern of VitC amphiphiles.

preparation of VitC amphiphiles was confirmed by ^{1}H nuclear magnetic resonance (^{1}H NMR, Fig. 1A) spectroscopy, ^{13}C nuclear magnetic resonance (^{13}C NMR, Fig. S1) spectroscopy and high-resolution mass spectrometry (HR-MS, Fig. 1B).

Then, the homogeneous supramolecular hydrogel was self-assembled by dissolving VitC amphiphiles in phosphate-buffered saline (PBS) with annealing treatment. The self-assembly behavior of hydrogel revealed an obvious concentration-dependent process, and the minimum gelation concentration (MGC) of VitC amphiphile was found to be 15 mM (Fig. S2). The morphology of the obtained hydrogel was characterized by transmission electron microscopy (TEM) imaging. A supramolecular nanofiber with entangled network was observed in Fig. 1C, indicating the successful self-assembly of VitC amphiphile. As shown in the enlarged TEM image, the compact filamentous nanostructures were clearly observed. Then, the mechanical properties of the hydrogel were evaluated by rheological analysis. In the detected concentration range in Fig. 1D and S3, the storage modulus (G′) of hydrogels was much higher than the loss modulus (G″), and both moduli were interdependent in the dynamic frequency sweep range, demonstrating the viscoelastic soft characteristic of the hydrogel. Moreover, as the concentration of hydrogel increased, both G′ and G″ increased significantly, indicating that more molecules participated in the self-assembly process to improve the mechanical properties of the hydrogel (Fig. S3a). Moreover, as shown in Fig. S3b, no temperature-induced phase transition was observed as G′ remained higher than G″ during the temperature sweep from 4 °C to 37 °C. Meanwhile, G′ and G″ increased initially and then remained stable until 20 °C, indicating that multiple noncovalent interactions including hydrophobic and hydrogen-bonding interactions reached a balanced state after 20 °C. Moreover, the VitC supramolecular hydrogel could quickly recover to its original shape and structure after being injected from needles with different gauge sizes due to its unique shear-thinning and self-healing properties (Fig. 1D and Fig. S4).

Subsequently, the self-assembly mechanism was investigated by Fourier transform infrared spectroscopy (FTIR) (Fig. 1E). The peaks of

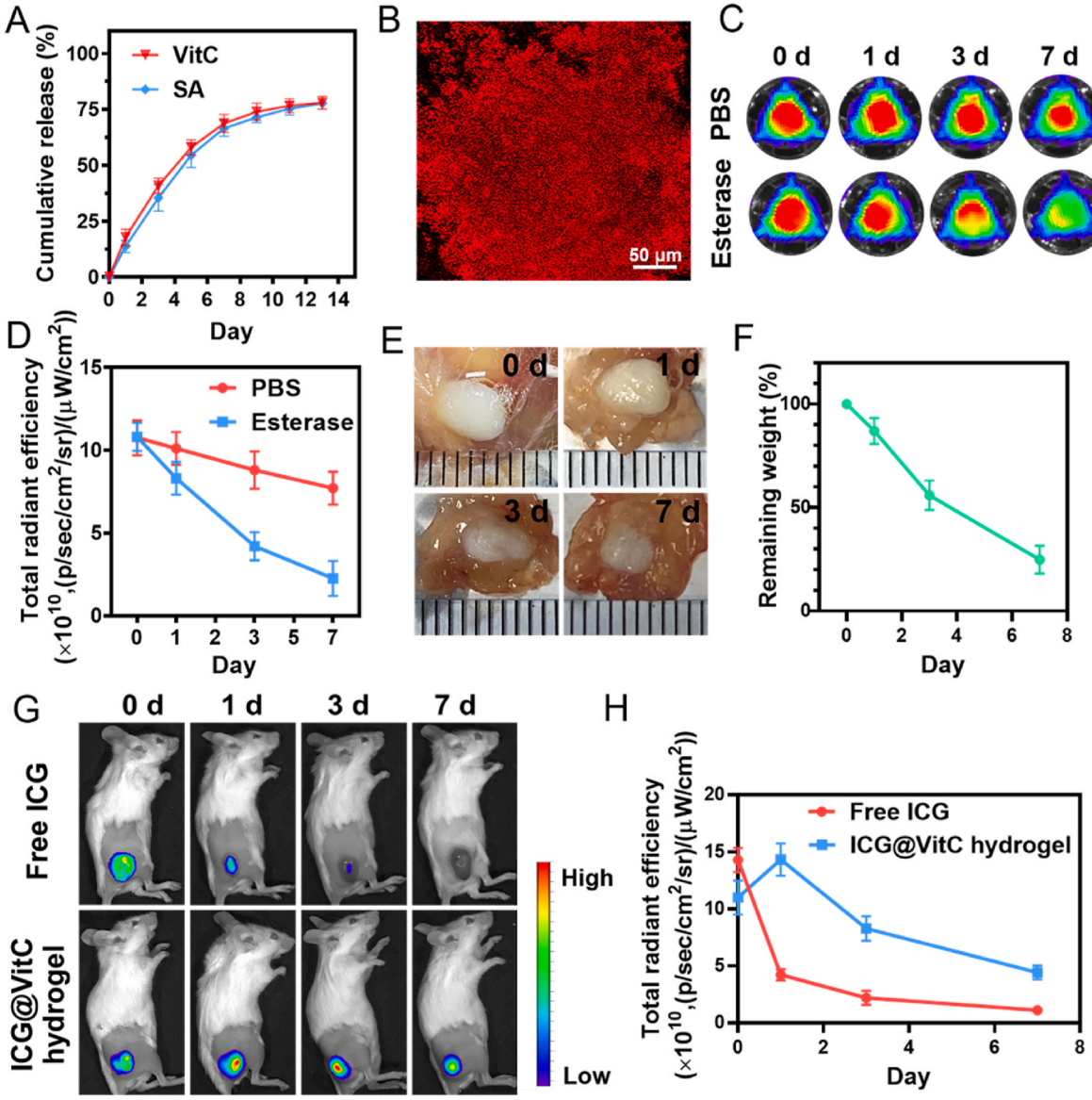

Fig. 2. Drug-release behavior of SA encapsulated VitC hydrogel. A) Cumulative release profiles of VitC and SA from the hydrogel in PBS with esterase. B) Representative confocal image of a cryosection of ICG-loaded hydrogel. C) Fluorescence images and D) related quantification analysis of ICG@VitC hydrogel in the transwell with or without esterase. E) Representative ex vivo photographs and F) remaining weight of VitC hydrogel after subcutaneous injection into the tumors of mice. G) Fluorescence imaging and H) quantified fluorescence signal in the tumors molecular packing model of mice injected with free ICG or ICG@VitC hydrogel. Data are presented as the mean ± SEM (n = 3).

asymmetric and symmetric stretching vibrations of CH_2 at 2923 and 2850 cm^{-1} shifted to lower wavenumbers at 2918 and 2848 cm^{-1}, demonstrating the ordered arrangement of lipid chains during the self-assembly process. Moreover, the polyhydroxy peak of VitC located above 3000 cm^{-1} became broad, and the peak at 3354 cm^{-1} shifted to 3334 cm^{-1}, illustrating the multiple and intense hydrogen bonds formed in the fibrous assemblies. As shown in the molecular packing model, the lipid chains were aggregated via hydrophobic interactions, and the

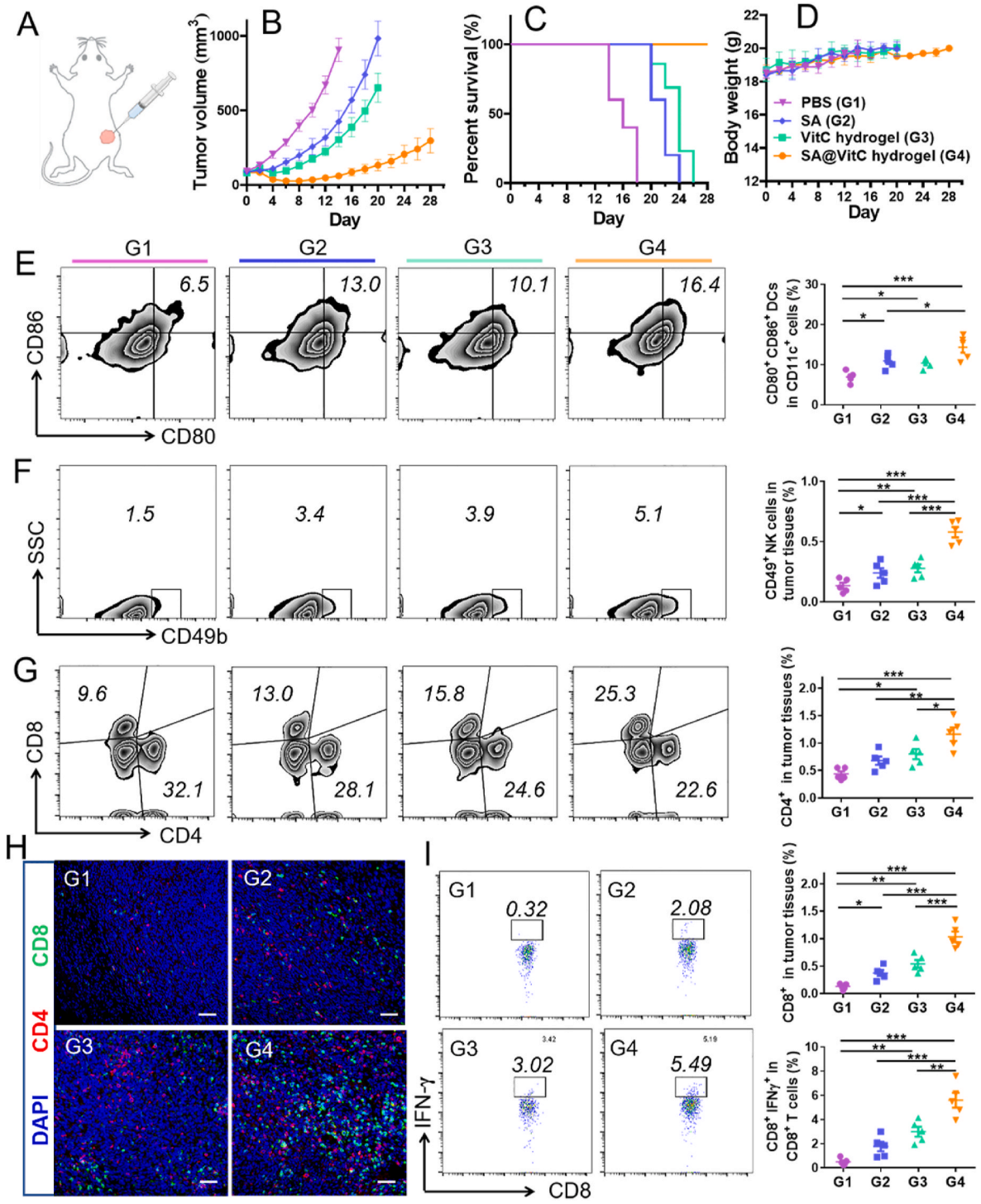

Fig. 3. Therapeutic results and immune responses induced by VitC-based hydrogel. A) Schematic illustrating the intratumor injection of hydrogel into mice bearing CT26 tumors. B) Average tumor-growth kinetics. The growth profile was stopped once the tumor volume of mice in this group exceeded 1000 mm^3. C) Survival curves corresponding to the tumor volume of mice in different groups. D) The weight of mice in different groups. E) Representative flow cytometry images (left) and relative quantification analysis (right) of $CD80^+CD86^+$ DCs in lymph nodes three days after different treatments. F and G) Representative flow cytometry images (left) and statistical analysis (right) of NK cells (gated on $CD45^+$) and T cells (gated on $CD3^+$) infiltrated in the tumor six days after different treatments. H) Immunofluorescence staining images of tumors showing the infiltration of $CD4^+$ and $CD8^+$ T cells. Scale bar, 50 μm. I) Flow cytometry images (left) and corresponding quantification analysis (right) of the percentage of $IFN\gamma^+CD8^+$ T cells in tumors after different treatments as indicated. All data are presented as the mean ± SEM ($n \geq 5$). Statistical significance was calculated via one-way ANOVA with a Tukey post hoc test. *$P < 0.05$; **$P < 0.01$; ***$P < 0.001$.

polyhydroxy headgroups interacted with each other by hydrogen-bonding interactions (Fig. 1F), which was consistent with the FTIR results.

Drug-release behavior of SA@VitC hydrogel. Then, the STING agonist SA (the molecular structure is provided in Fig. S5), which has been proposed to enhance tumor immunogenicity was encapsulated to form the SA@VitC hydrogel. It was found that the encapsulation of SA exhibited negligible effects on the formation and structure of the VitC hydrogel (Fig. S6). Then, the release behaviors of SA and VitC from the SA@VitC hydrogel were assessed in PBS containing esterase (50.0 units/mL) at 37 °C. As observed in Fig. 2A, SA and VitC were quickly released in the presence of esterase in the initial 7 days with cumulative release over 60%, and the release rate was gradually reduced in the subsequent time period. Additionally, the cumulative release behaviors of VitC amphiphile and VitC from VitC hydrogel in the absence of esterase were also studied (Fig. S7). As expected, nearly no VitC was detected and VitC amphiphile showed similar release mode with that of VitC in the presence of esterase, indicating that VitC hydrogel would disassemble in the dialysate, and then VitC amphiphile could be more accessible to esterase, leading to sustainable release of both VitC and encapsulated SA [43–45]. Next, a fluorescence dye, indocyanine green (ICG), was encapsulated in the amphiphilic matrix to form the ICG@VitC hydrogel for more intuitive observation. As shown in the confocal images of the frozen sections of ICG@VitC hydrogel, the fluorescence signal from ICG exhibited uniform distribution in the gel, indicating the successful encapsulation of cargos in the hydrogel matrix (Fig. 2B). Then, the release of encapsulated agent in VitC hydrogel in PBS with or without esterase was further studied. The fluorescence signal of ICG from the VitC hydrogel dispersed in PBS containing esterase lost much more quickly than that dispersed in PBS, further confirming that esterase could promote the degradation of VitC hydrogel and lead to the quick release of encapsulated cargos (Fig. 2C and D).

We then investigated the degradation behavior of VitC hydrogel *in vivo*. VitC hydrogel (1% (w/v), 100 μL) was subcutaneously injected into the backs of Balb/c mice, and then the mice were sacrificed, and the remaining hydrogel was photographed and weighed at the indicated time points (Fig. 2E and F). The nearly linear weight loss profile of VitC hydrogel confirmed its degradation behavior *in vivo* (Fig. 2F). To investigate the sustained release of encapsulated drugs from this VitC hydrogel, ICG-loaded VitC hydrogel and free ICG solution were injected into the tumors of mice and imaged by an *in vivo* fluorescence imaging system. As shown in Fig. 2G and H, the fluorescence signal of ICG in the tumor injected with ICG@VitC hydrogel was obviously detected even 7 days after injection, while the signal of ICG in the tumor injected with free ICG rapidly disappeared one day later. Quantitative statistical analysis further demonstrated the sustained release of ICG in tumors with ICG@VitC hydrogel injection. Therefore, the VitC hydrogel could be employed as a reservoir for targeted and long-term drug delivery.

Immunotherapy and immune responses induced by SA@VitC hydrogel. Encouraged by the slow degradation and sustained release of encapsulated agents from VitC hydrogel, we then evaluated the anti-tumor effects of SA@VitC hydrogel on the subcutaneous CT26 colon tumor model (Fig. 3A). After CT26 tumors implanted, mice were grouped and intratumorally injected with PBS (20 μL), free SA (15 μg per mouse, 20 μL), VitC hydrogel (2.5% (w/v), 20 μL) or SA@VitC hydrogel (15 μg SA per mouse, 2.5% (w/v) VitC hydrogel, 20 μL). Compared to the PBS group, the VitC hydrogel itself delayed tumor growth and extended the life span to 20–26 days, indicating that VitC at a high local concentration indeed exerted antitumor effects (Fig. 3B, C and Fig. S8). Moreover, the mice treated with SA@VitC hydrogel showed the smallest tumor volume (Fig. 3B) and significantly prolonged survival to 100% within four weeks (Fig. 3C) due to the encapsulation of STING agonist SA, which could promote the immune-stimulating tumor microenvironment and augment antitumor immune responses [46–48]. These results suggested that the SA@VitC hydrogel was able to sustainably release SA and VitC during degradation, and that the released VitC may regulate the immune microenvironment to promote the immune responses induced by SA. Meanwhile, to investigate whether the injectable hydrogel could cause mechanical damage to tumors, a control group, calcium ion coordinated alginate hydrogel (Ca@ALG hydrogel) was added. As shown in Fig. S9, compared to the PBS group, the growth rate of tumors injected with Ca@ALG remained nearly unchanged, but the growth rate of tumors injected with VitC hydrogel was obviously inhibited, indicating that the mechanical damage induced by injectable hydrogel could not delay the growth of tumors. Thus, the SA@VitC hydrogel could achieve a synergistic therapeutic effect. In addition, no appreciable decrease in body weight was observed, suggesting that such locally applied SA@VitC hydrogel induced no obvious side effects (Fig. 3D).

Then, we investigated the population of different immune cells infiltrated in the tumor with different treatments. We first investigated the maturation of DCs, which are critical antigen-presenting cells connecting the innate and adaptive immune systems [49]. Three days-after different treatments, the tumors near lymph nodes were collected to obtain single cells for flow cytometry analysis. Compared to the PBS group, both free SA and VitC hydrogel could promote DC maturation (Fig. 3E). More excitingly, the percentage of DC maturation (16.4%) of SA-loaded VitC hydrogel was higher than that treated with VitC hydrogel (10.1%) or free SA (13.0%), demonstrating that SA-encapsulated VitC hydrogel could synergistically promote DC maturation. In the parallel experiment, six days after different treatments, the mice were sacrificed, and their tumors were collected to analyze different immune cells by flow cytometry. Notably, the percentage of tumor-infiltrating natural killer (NK) ($CD45^+CD49b^+$) cells was increased in VitC hydrogel- and SA@VitC hydrogel-treated tumors, indicating that both SA and VitC hydrogel were effective in activating NK cells (Fig. 3F). In addition to NK cells, we further studied the percentage of T cells, which usually play an important role in inhibiting tumor growth. Strikingly, the percentages of tumor-infiltrating $CD4^+$ ($CD3^+CD4^+CD8^-$) and $CD8^+$ ($CD3^+CD4^-CD8^+$) T cells, especially interferon-γ-positive $CD8^+$ ($CD3^+CD8^+IFN\text{-}\gamma^+$) T cells, obviously increased in SA@VitC hydrogel-treated tumors, further demonstrating that SA-encapsulated VitC hydrogel could synergistically boost the adaptive immune system (Fig. 3G and I). In addition to the results measured by flow cytometry, immunofluorescence staining of tumor slides collected from mice with different treatments visually indicated that SA@VitC hydrogel obviously increased the infiltration of $CD4^+$ and $CD8^+$ T cells in the tumor (Fig. 3H).

In addition to investigating the percentage of different immune cells within the tumor, we also studied the concentration of different cytokines six days after different treatments. As observed in Fig. 4A, the levels of tumor necrosis factor α (TNF-α) and interferon-γ (IFN-γ) in the sera of mice in both VitC hydrogel and SA@VitC hydrogel groups were increased (Fig. 4A). Considering that SA is a STING agonist that can trigger the production of type I IFNs [15] we then measured the production of type I IFNs through costimulatory markers IFN-β and C-X-C motif chemokine ligand 10 (CXCL10) by quantitative real-time polymerase chain reaction (q-PCR) assay. As we expected, the induction of IFN-β and CXCL10 transcripts was obviously observed after SA@VitC hydrogel treatment, indicating the successful activation of the STING pathway (Fig. 4B). In contrast, free SA slightly induced the transcription of IFN-β and CXCL10, which may be due to the quick release of free SA. Thus, the SA@VitC hydrogel exhibited obviously enhanced ability to activate the STING pathway due to the sustained release of SA delivered by VitC hydrogel.

Encouraged by the above results, we further evaluated the mechanism of such strong immune responses induced by the VitC hydrogel itself. According to previous papers, high-dose VitC could act as a cofactor for a family of gene regulatory enzymes to effectively activate various immune cells and improve the immunogenicity of tumors.[7-12] Thus, we then investigated the effect of VitC on two important immune cells, DCs and $CD8^+$ T cells *in vitro*. To study the effect of VitC on DC

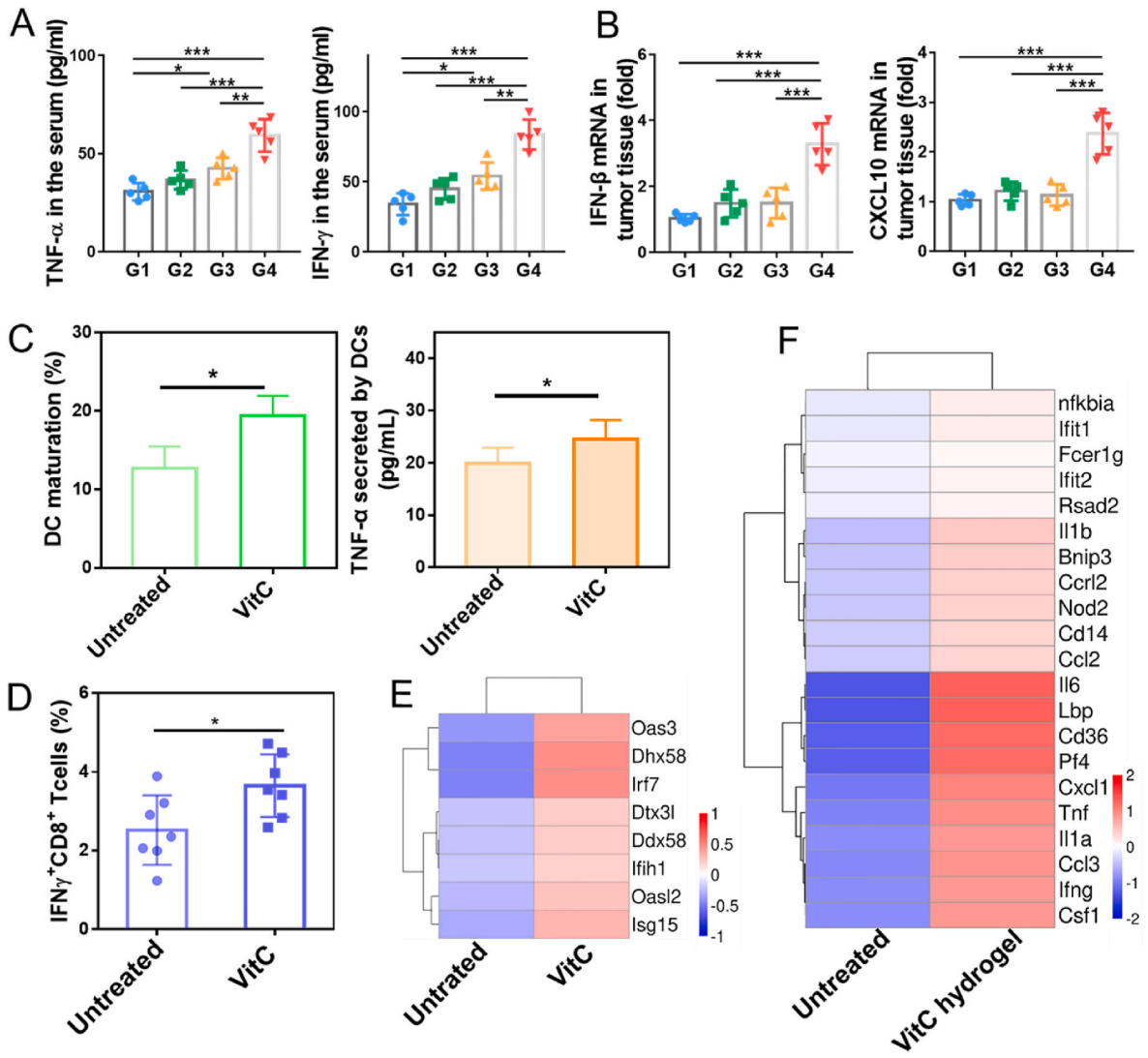

Fig. 4. Immune responses and related mechanism induced by SA@VitC hydrogel. The levels of A) TNF-α and IFN-γ in the serum and B) IFN-β and CXCL10 in the tumor isolated six days after different treatments. C) Maturation of BMDCs measured by flow cytometry (left) and the level of TNF-α secreted by BMDCs (right) evaluated by ELISA. D) Flow cytometry analysis of the percentage of $IFN\gamma^+CD8^+$ T cells. BMDCs and $CD8^+$ T cells were pretreated with or without 1 mM VitC for 12 h. Then, BMDCs were further incubated in fresh media for 24 h, and $CD8^+$ T cells were further incubated in fresh media for 12 h for measurement. E & F) Heatmap of differentially expressed genes of E) VitC (1 mM)-treated CT26 cells and F) VitC hydrogel (2.5% (w/v)-treated tumors as assessed by RNA sequencing. G1, PBS; G2, SA; G3, VitC hydrogel; G4, SA@VitC hydrogel. All data are presented as the mean ± SEM (n ≥ 5). Student's *t*-test and one-way ANOVA with a Tukey post hoc test were used for two-group and multiple comparisons, respectively. P value style: *p < 0.05; **p < 0.01; ***p < 0.001.

maturation, bone marrow-derived DCs (BMDCs) were incubated with different concentrations of VitC, and the maturation of BMDCs was measured by detecting the surface expression of costimulatory molecules CD80 and CD86. It was observed that VitC at concentrations higher than 1 mM significantly promoted DC maturation (Figs. S10–S11 & Fig. 4C). Then, the concentration of tumor necrosis factor-α (TNF-α) secreted by BMDCs after incubation with 1 mM VitC was measured. Interestingly, the concentration of TNF-α was also obviously increased in VitC-treated group (Fig. 4C), indicating that VitC at suitable concentrations could indeed directly promote DC maturation. In addition, we also found that $CD8^+$ T cells isolated from the spleen of mice after co-incubation with VitC *in vitro*, exhibited a higher percentage of $IFN\gamma^+$ $CD8^+$ T cells (Fig. 4D and Fig. S12), suggesting that VitC may promote lymphocyte activation.

In addition to immune cells, we also carried out transcriptome sequencing analysis of CT26 cancer cells after incubation with VitC. As shown in Fig. 4E, CT26 cancer cells incubated with VitC exhibited upregulated expression of many endogenous viral defense genes, which could promote the recognition of tumor cells by immune system. Moreover, we further carried out transcriptome sequencing analysis of CT26 tumors three days after injection with VitC hydrogel (2.5% (w/v), 20 μL). As shown in Fig. 4F, the genes related to viral recognition and defense, IFN signaling and apoptotic signaling were markedly upregulated in VitC hydrogel-treated tumor cells. To investigate whether the pro-oxidative effects of VitC at high concentrations would contribute to antitumor immunotherapy, the level of reactive oxygen species (ROS) in the tumor tissue was analyzed using a 2′,7′-dichlorofluorescein diacetate (DCFH-DA) probe. As shown in the fluorescence imaging, no detectable difference was found in the tumor slides collected from mice treated with VitC hydrogel and PBS (Fig. S13). Taken together, these results indicated that the VitC hydrogel activated the immune system by engaging in multiple immune stimulation pathways. Although more detailed data are still necessary to reveal these mechanisms, our pilot study indeed provided presumptive positive evidence for VitC-based hydrogels to promote cancer immunotherapy.

Distant tumor inhibition effect. We further assessed whether such

immune effects induced by the locally applied SA@VitC hydrogel could inhibit the growth of distant tumors. As exhibited in Fig. 5A, a bilateral CT26 tumor model was established in this experiment. A first tumor implanted on the right side of each mouse was defined as the "primary tumor", and a second tumor inoculated four days later on the left side was called the "distant tumor". This tumor model was established by many other works to evaluate the systemic immune responses [50–52]. After the indicated treatment of the primary tumors, the sizes of tumors on both sides were measured every two days. Excitingly, both VitC hydrogel and free SA not only inhibited the growth of primary tumors but also suppressed the development of distant tumors. As expected, thanks to the long-term retention and sustained release of VitC and SA from VitC hydrogel, the sizes of both primary and distant tumors in SA@VitC hydrogel-treated group were much smaller than those in other groups at all time points (Fig. 5B). The impairment of distant tumors was further identified by a terminal deoxynucleotidyl transferase-mediated dUTP-biotin nick end labeling (TUNEL) assay. As shown in Fig. 5C, apparent apoptosis was detected in the distant tumors collected from mice treated with SA@VitC hydrogel.

To reveal the abscopal tumor inhibition mechanism induced by locally applied SA@VitC hydrogel, distant tumors were collected to evaluate different immune cells by flow cytometry. Compared to PBS group, different immune cells, including NK cells and $CD8^+$ T cells, in the distant tumors collected from mice in SA@VitC hydrogel-treated

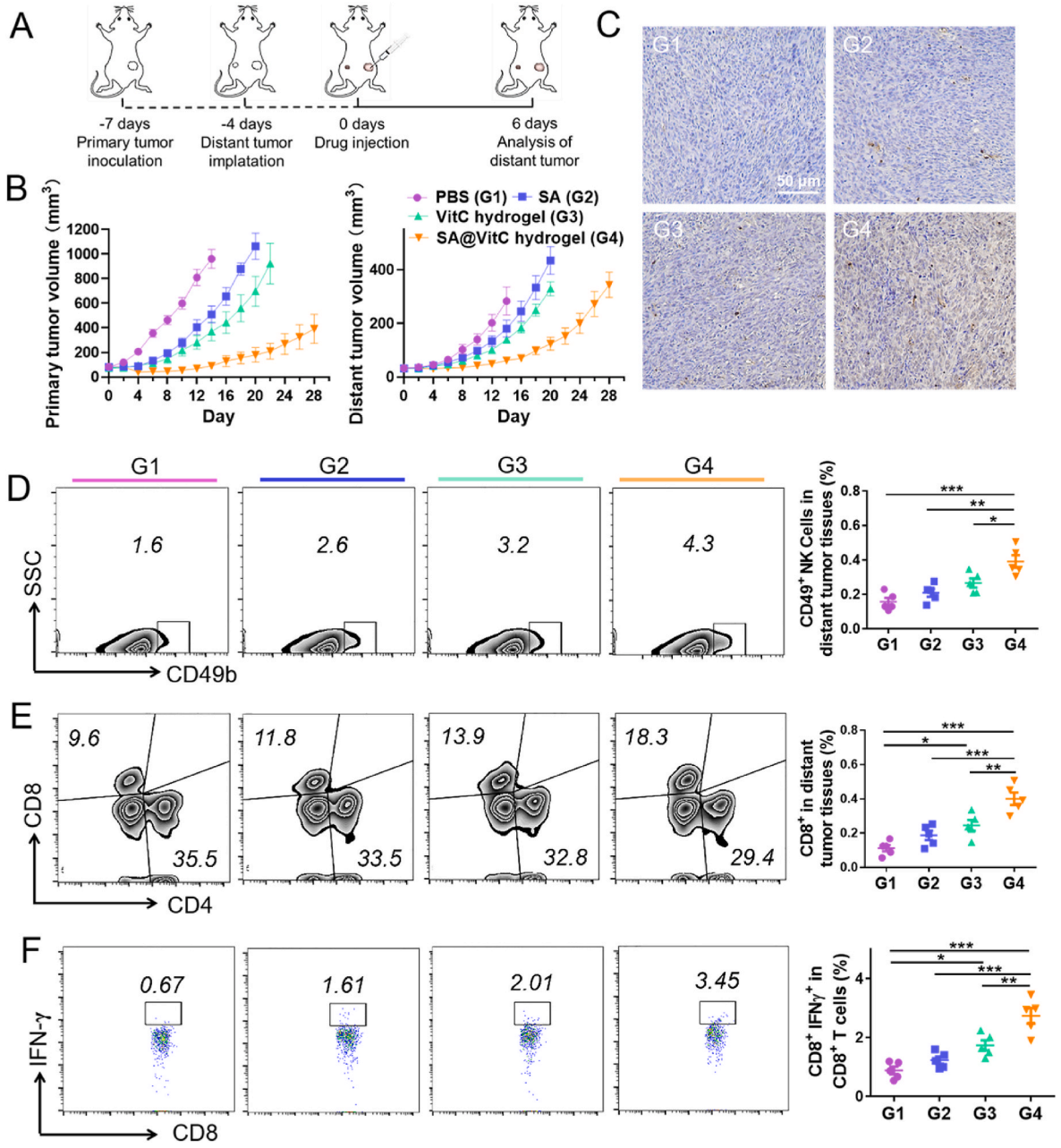

Fig. 5. Systemic antitumor immune responses induced by locally applied VitC hydrogel. A) Schematic illustrating the therapy in the bilateral CT26 tumor model. Tumors on the right side were designated primary tumors with treatment, and tumors on the left side were designated distant tumors without any treatment. B) Tumor growth kinetics of both primary and distant tumors. C) TUNEL staining of distant tumor slides. D and E) Flow cytometry analysis of the percentage of infiltrated NK and $CD8^+$ T cells in distant tumors in different groups. F) Flow cytometry analysis of the percentage of $IFN\gamma^+CD8^+$ T cells in distant tumors in different groups. All data are presented as the mean ± SEM (n = 5). Statistical significance was calculated via one-way ANOVA with a Tukey post hoc test. *P* value style: *p < 0.05; **p < 0.01; ***p < 0.001.

group were obviously increased (Fig. 5D and E). Moreover, the activation of T cells in the distant tumors was further confirmed by the improved percentage of IFNγ$^+$CD8$^+$ T cells in SA@VitC hydrogel group (Fig. 5F). Taken together, these results suggested that the locally applied SA@VitC hydrogel could effectively activate the systemic immune system to trigger strong protective immune responses against abscopal tumors, exhibiting great potential in killing metastatic tumors.

2. Conclusions

Here, we have developed a novel nanofiber hydrogel that is self-assembled by esterase-sensitive VitC amphiphiles for enhanced cancer immunotherapy. It was found that such VitC supramolecular hydrogels with unique self-healing properties could be injected into the tumor and act as a reservoir for targeted and sustained release of VitC in the tumor. Moreover, this VitC hydrogel also acted as an effective delivery platform for other immunotherapeutics, such as STING agonist-4 (SA). Interestingly, the self-delivery VitC nanofiber hydrogel itself could inhibit CT26 tumor growth by upregulating genes related to IFN signaling and apoptotic signaling, together with viral recognition and defense. More importantly, the SA@VitC hydrogel with the ability to activate these antitumor and STING pathways could significantly promote DC maturation and improve the tumor infiltration of NK cells and T cells, leading to serious tumor regression and systemic immune surveillance. Our findings emphasized that the localized VitC nanofiber hydrogel offers great potential to sensitize tumors to immunotherapy in a highly effective and safe manner, which will accelerate the clinical development of VitC-based cancer immunotherapy.

3. Experimental section

Materials, cell lines, and animals. Vitamin C (VitC), dodecyl isocyanate, acetyl chloride and benzyl bromide (BnBr) were purchased from Alfa Aesar. Hexane, dichloromethane (DCM), acetonitrile, ethyl acetate (EA), triethylamine (TEA), and methanol (MeOH) were obtained from 3A Chem. STING agonist-4 (SA) was purchased from MedChemExpress. Catalase solution (≥35,000 units per mg protein) was obtained from Aladdin. Ascorbic acid assay kit was purchased from BioVision. All other reagents, if not specified, were acquired from Sigma Aldrich and used without additional purification. Mouse colon cancer CT26 cells obtained from American Type Culture Collection (ATCC) were cultured in 1640 medium (Gibco, Invitrogen) supplemented with 10% premium fetal bovine serum (Gibco) and 1% penicillin−streptomycin (Gibco) in an incubator containing 5% CO_2 at 37 °C. Female Balb/c mice (6–8 weeks) were purchased from Nanjing Pengsheng Biological Technology Co. All animal experiments complied with the animal protection laws of China and were approved by Soochow University Laboratory Animal Center (No. ECSU-2019000198).

Synthesis of VitC amphiphile. The synthesis route of VitC amphiphiles is shown in Fig. S1. 5,6-*O,O*-Isopropylidene VitC (1), 2,3-*O,O*-dibenzyl-5,6-*O,O*-isopropylidene VitC (2) and 2,3-*O,O*-dibenzyl VitC (3) were synthesized with procedures reported in previous literature [41, 42]. Dibenzyl VitC derivative 3 (1 g, 2.8 mmol) and TEA (1 mL) were dissolved in DCM (30 mL) at 0 °C. Then, dodecyl isocyanate (0.65 g, 3.07 mmol) was added dropwise, and the reaction mixture was stirred overnight at room temperature (rt). Then, the solvent was removed, and the mixture was further purified by column chromatography (EA/hexane = 1/3) on silica gel to obtain VitC derivative 4 as a yellowish oil (1.02 g, 64.1% yield).

Next, VitC derivative 4 (280 mg, 0.5 mmol) was dissolved in a mixed solution of EA/MeOH (15 mL, V/V = 1/4). Following the addition of 10% Pd/C (14 mg), the mixture was stirred at rt overnight in a hydrogen atmosphere. Next, Pd/C was removed by filtration, and the filtrate was concentrated to obtain VitC amphiphiles as white powder (135 mg, 69.6% yield). ^{1}H NMR (600 MHz, DMSO-d_6) δ (ppm): δ 11.09 (s, 1H), 8.38 (s, 1H), 7.16 (t, J = 5.6 Hz, 1H), 5.21 (s, 1H), 4.63 (s, 1H), 4.02–4.00 (m, 1H), 3.95–3.91 (m, 2H), 2.97–2.93 (m, 2H), 1.39–1.37 (m, 2H), 1.28–1.13 (m, 18H), 0.85 (t, J = 6.6 Hz, 3H). ^{13}C NMR (151 MHz, DMSO-d_6) δ (ppm): 170.8, 156.3, 152.6, 118.6, 75.4, 66.3, 64.8, 40.7, 31.7, 29.8, 29.5, 29.4, 29.2, 29.1, 26.7, 22.53, 14.4. HRMS (*m/z*, ESI): calcd for $C_{19}H_{34}NO_7$ $[M+H]^+$ 388.2335, found 388.2312; calcd for $C_{19}H_{34}NO_7$ $[M+Na]^+$ 410.2155, found 410.2136.

Preparation and characterization of VitC hydrogel. To prepare the VitC hydrogel, VitC amphiphiles (20 mg/mL) in phosphate buffered saline (PBS, 10 mM) were heated to 60 °C until a homogeneous solution appeared. The formation of VitC hydrogel by self-assembly took place during the cooling process. To fabricate the drug-loaded hydrogel, free SA or indocyanine green (ICG) solution was mixed into VitC solution before self-assembly. The hydrogel was stored at 4 °C before use and returned to room temperature (25 °C) before use. TEM imaging of the hydrogel was obtained using an FEI Tecnai F20 transmission electron microscope. Then, the rheological test of the VitC hydrogel was carried out on an AR 2000ex (TA Instruments) system. The parallel plates used for the test were 25 mm, and the gap during the experiment was 500 μm. A VERTEX-70/70v spectrometer (Bruker Optics, Germany) was used to execute FTIR characterization. The fluorescence image of the cryosection of the ICG-loaded hydrogel was acquired using a confocal laser scanning microscope (Zeiss LSM 710).

Drug release behavior from VitC hydrogel. The release behavior of SA from the VitC hydrogel was assessed under sink conditions in PBS containing porcine liver esterase (50.0 units/mL) and NaN_3 (0.2 wt%) at 37 °C. At the indicated time points, 0.5 mL dialysate was collected and replaced with the same volume of fresh medium. The quantity of released SA was determined using high-performance liquid chromatography (HPLC, BioLogical DuoFlowTM). To visually observe the release behavior of the drug from the VitC hydrogel, the fluorescent dye ICG was loaded in the hydrogel. Then, the hydrogel (150 μL) was placed into the upper chamber of a Transwell plate (pore size = 8 μm, Corning, cat. No. 3422), and PBS with or without esterase was added to the bottom of the chamber. The fluorescence images of the upper chambers were imaged by an IVIS Spectrum Imaging System (PerkinElmer) at different time points. Regions of interest were quantified as total radiant efficiency [p/s]/[μW/cm^2] (IVIS Living Image 4.2).

Immunoregulation properties of VitC *in vitro*. Bone marrow-derived dendritic cells (BMDCs) were collected from the bone marrow of naive Balb/c mice and incubated with granulocyte macrophage-colony stimulating factor (GM-CSF) for seven days until their blank maturation rate was approximately 20% for future use. Splenocytes were obtained from Balb/c mice to separate T cells using the MACS pan T cell Isolation Kit (Miltenyi Biotec, Germany) following the manufacturer's instructions. The isolated T cells were cultured in specific medium containing anti-CD3 (5 μg/mL), anti-CD28 (1 μg/mL) and IL-2 (10 μg/mL) for proliferation. Prior to treatment with high-dose VitC *in vitro*, cells were exposed to catalase to quench free radicals as previously suggested. Briefly, all the cells were pretreated with catalase (100 μg/mL) for 1 h and then cultured in medium with or without VitC for another 12 h. After the treatment, the cells were washed and resuspended in fresh medium for assessment.

Hydrogel degradation and drug release behavior *in vivo*. VitC hydrogel (100 μL) was injected into the backs of Balb/c mice, and then the mice were euthanized at predetermined time points. The remaining hydrogel in each mouse was photographed, and the amount of remaining gelator was determined by HPLC. For *in vivo* fluorescence imaging, the same volume of free ICG or ICG-loaded hydrogel (20 μL, equivalent ICG concentration at 0.2 mg/mL) was intratumorally injected into CT26 mouse colon tumor–bearing mice (n = 4). The signals were monitored by an IVIS Spectrum Imaging System at the indicated time points.

***In vivo* tumor models and treatments.** CT26 cells (1×10^6 cells, 50 μL) were subcutaneously injected into the backs of female Balb/c mice to establish the primary tumor. Mice were randomly divided into four groups (n = 5) until the tumor size reached ~80 mm^3 and then treated

with PBS, free SA, VitC hydrogel and SA@VitC hydrogel (SA = 15 μg, VitC gelator = 0.5 mg per mouse). For inoculation of distant tumors, 1.0×10^6 CT26 cells were inoculated into the left flank of each mouse four days after implanting the primary tumor. The tumor volume was calculated according to the formula: tumor volume = length × width^2/2. Mice were euthanized when their tumor volume exceeded 1000 mm^3.

Flow cytometry analysis. The tumor tissues resected from mice were sliced into small pieces, digested and filtered to form single-cell suspensions. The cells were counted and divided into 10^5 cells/tube and then stained with fluorescence-labeled antibodies, including anti-CD45 (cat. No. 103108), anti-CD49b (cat. No. 103516), anti-CD80 (cat. No. 104714), anti-CD86 (cat. No. 105008), anti-CD3 (cat. No. 100204), anti-CD4 (cat. No. 100412), anti-CD8 (cat. No. 100708), and anti–IFN–γ (cat. No. 505810) according to the manufacturer's instructions for flow cytometry analysis on a C6 plus flow cytometer. All data were analyzed by FlowJo software (Ver. 10.0.7).

Cytokine detection. Serum samples were isolated from mice 6 days after different treatments. The concentrations of TNF-α (eBioscience) and IFN-γ (eBioscience) were measured by enzyme-linked immunosorbent assay (ELISA) kits following the manufacturer's instructions. To detect the levels of IFN-β and CXCL-10, RNA was collected and transcribed into complementary DNA (cDNA) with a RevertAid First Strand cDNA Synthesis Kit (Thermo). Quantitative RT–PCR was performed using FastStart Universal SYBR Green Master Mix (Rox) (Servicebio) by StepOne Plus (ABI) in accordance with the instructions provided by the manufacturer. The following primers were used (5′→3′): M-GAPDH-S, CCTCGTCCCGTAGACAAAATG, M-GAPDH-A, TGAGGTCAATGAAGGGG TCG-T, M-IFNB-S, GAGTTACACTGCCTTTGCCATC, M-IFNB-A, CAAGTG GAGAGC-AGTTGAGGAC, M-CXCL10-S, TGCCTCATCCTGCTGGGTCT, M-CXCL10-A, and GCTCATCATTCTTTTTCATCGTGG. RNA expression was normalized to GAPDH expression in the relevant untreated control.

Immunofluorescence staining. Tumors harvested from the mice were cryo-embedded in optimum cutting temperature compound and sectioned into 10-μm-thick slices using a cryotome at −25 °C. Then, the tumor sections were stained with different primary antibodies: anti-CD4 (Abcam, cat. No. ab183685), anti-CD8 (Abcam, cat. No. ab22378) overnight at 4 °C. After washing in PBS 5 times, the slices were stained with fluorescently labeled goat anti-rat IgG (H + L; Thermo Fisher Scientific, cat. No. A18866) according to the vendors' protocols. In addition, the reactive oxygen species (ROS) in tumor tissue were stained with a 2′,7′-dichlorofluorescein diacetate (DCFH-DA) probe and imaged by confocal microscopy.

Histological investigation. Tissues were harvested, fixed in 4% paraformaldehyde, embedded in paraffin, and sectioned at a thickness of 10 μm. Standard hematoxylin and eosin (H&E) staining was performed on tumor sections according to the manufacturer's protocol. TUNEL staining was performed using a DNA fragmentation detection kit (S7101, Millipore, USA). All results were observed by optical microscopy (Leica, DM4000).

Statistical analysis. All data are shown as the mean ± standard error of the mean (s.e.m.). Student's *t*-test and one-way ANOVA with a Tukey post hoc test were used for two-group and multiple comparisons, respectively. Survival benefit was assessed using a log-rank test. The threshold for statistical significance was *P < 0.05; **P < 0.01; ***P < 0.001. Statistical analysis was performed via GraphPad Prism software 7.

4. Associated content

Supporting Information: Synthesis route of VitC amphiphile; ^{13}C NMR spectrum of VitC amphiphile; The self-assembly behavior of VitC gelator; Rheological properties of VitC hydrogels; Injectability of VitC hydrogel; Chemical structure of SA; TEMimage of SA@VitC hydrogel; Cumulative release profiles of VitC amphiphile and VitC from VitC hydrogel; Individual tumor-growth kinetics; Average tumor-growth kinetics; The maturation of DCs treated with VitC at different concentrations; Representative flow cytometric analysis images of DC maturation; Representative flow cytometric analysis images of IFNγ$^+$CD8$^+$ T cells isolated from the spleen; ROS level of tumor measured by DCFH-DA.

Credit Author Statement

Han Zhang and Qian Chen designed the research; Han Zhang, Yimou Gong, Wenjun Zhu, Jiafei Zhu, and Feng Pan performed the experiments; Han Zhang, Kai Liu, Zhishen Xiao, Yang Yang, and Qian Chen analyzed the data; and Han Zhang, Yang Yang and Qian Chen wrote the paper with constant feedback and comments from other authors and lab members. All authors contributed to the final draft.

Declaration of competing interest

The authors declare no conflict of interest.

Data availability

Data will be made available on request.

Acknowledgements

This work was partially supported by the National Research Programs of China (2020YFA0211100), the National Natural Science Foundation of China (91959104, 21927803, 51903182, 51525203, 52103347, 52032008), the Natural Science Foundation of Jiangsu Province (BK20190826), the China Postdoctoral Science Foundation (2020M671583), Suzhou Key Laboratory of Nanotechnology and Biomedicine, Collaborative Innovation Center of Suzhou Nano Science and Technology, and the 111 Program from the Ministry of Education of China.

Appendix A. Supplementary data

Supplementary data to this article can be found online at https://doi.org/10.1016/j.biomaterials.2022.121673.

References

[1] N. Shenoy, E. Creagan, T. Witzig, M. Levine, Ascorbic acid in cancer treatment: let the phoenix fly, Cancer Cell 34 (2018) 700–706.
[2] M. Agathocleous, C.E. Meacham, R.J. Burgess, E. Piskounova, Z. Zhao, G.M. Crane, B.L. Cowin, E. Bruner, M.M. Murphy, W. Chen, G.J. Spangrude, Z. Hu, R. J. DeBerardinis, S.J. Morrison, Ascorbate regulates haematopoietic stem cell function and leukaemogenesis, Nature 549 (2017) 476–481.
[3] M. Di Tano, F. Raucci, C. Vernieri, I. Caffa, R. Buono, M. Fanti, S. Brandhorst, G. Curigliano, A. Nencioni, F. de Braud, V.D. Longo, Synergistic effect of fasting-mimicking diet and vitamin C against KRAS mutated cancers, Nat. Commun. 11 (2020) 2332.
[4] B. Ngo, J.M. Van Riper, L.C. Cantley, J. Yun, Targeting cancer vulnerabilities with high-dose vitamin C, Nat. Rev. Cancer. 19 (2019) 271–282.
[5] Y. Ma, J. Chapman, M. Levine, K. Polireddy, J. Drisko, Q. Chen, High-dose parenteral ascorbate enhanced chemosensitivity of ovarian cancer and reduced toxicity of chemotherapy, Sci. Transl. Med. 6 (2014) 222ra18. -222ra18.
[6] R.A. Luchtel, T. Bhagat, K. Pradhan, W.R. Jacobs, M. Levine, A. Verma, N. Shenoy, High-dose ascorbic acid synergizes with anti-PD1 in a lymphoma mouse model, Proc. Natl. Acad. Sci. 117 (2020) 1666–1677.
[7] K. Blaschke, K.T. Ebata, M.M. Karimi, J.A. Zepeda-Martínez, P. Goyal, S. Mahapatra, A. Tam, D.J. Laird, M. Hirst, A. Rao, M.C. Lorincz, M. Ramalho-Santos, Vitamin C induces Tet-dependent DNA demethylation and a blastocyst-like state in ES cells, Nature 500 (2013) 222–226.
[8] A. Magrì, G. Germano, A. Lorenzato, S. Lamba, R. Chilà, M. Montone, V. Amodio, T. Ceruti, F. Sassi, S. Arena, S. Abrignani, M. D'Incalci, M. Zucchetti, F. Di Nicolantonio, A. Bardelli, High-dose vitamin C enhances cancer immunotherapy, Sci. Transl. Med. 12 (2020), eaay8707.
[9] J. Yun, E. Mullarky, C. Lu, K.N. Bosch, A. Kavalier, K. Rivera, J. Roper, I.I.C. Chio, E.G. Giannopoulou, C. Rago, A. Muley, J.M. Asara, J. Paik, O. Elemento, Z. Chen, D.J. Pappin, L.E. Dow, N. Papadopoulos, S.S. Gross, L.C. Cantley, Vitamin C selectively kills KRAS and BRAF mutant colorectal cancer cells by targeting GAPDH, Science 350 (2015) 1391–1396.

[10] A. Ang, J.M. Pullar, M.J. Currie, M.C.M. Vissers, Vitamin C and immune cell function in inflammation and cancer, Biochem. Soc. Trans. 46 (2018) 1147–1159.
[11] Y.-J. Jeong, J.-H. Kim, J.-M. Hong, J.S. Kang, H.-R. Kim, W.J. Lee, Y. Hwang, Vitamin C treatment of mouse bone marrow-derived dendritic cells enhanced CD8 + memory T cell production capacity of these cells in vivo, Immunobiology 219 (2014) 554–564.
[12] M. Liu, H. Ohtani, W. Zhou, A.D. Ørskov, J. Charlet, Y.W. Zhang, H. Shen, S. B. Baylin, G. Liang, K. Grønbæk, P.A. Jones, Vitamin C increases viral mimicry induced by 5-aza-2′-deoxycytidine, Proc. Natl. Acad. Sci. 113 (2016) 10238–10244.
[13] V. Sasidharan Nair, M.H. Song, K.I. Oh, Vitamin C facilitates demethylation of the Foxp3 enhancer in a tet-dependent manner, J. Immunol. 196 (2016) 2119–2131.
[14] K.B. Chiappinelli, P.L. Strissel, A. Desrichard, H. Li, C. Henke, B. Akman, A. Hein, N.S. Rote, L.M. Cope, A. Snyder, V. Makarov, S. Buhu, D.J. Slamon, J.D. Wolchok, D.M. Pardoll, M.W. Beckmann, C.A. Zahnow, T. Merghoub, T.A. Chan, S.B. Baylin, R. Strick, Inhibiting DNA methylation causes an interferon response in cancer via dsRNA including endogenous retroviruses, Cell 162 (2015) 974–986.
[15] M. Levine, S.J. Padayatty, M.G. Espey, Vitamin C: a concentration-function approach yields pharmacology and therapeutic discoveries, Adv. Nutr. 2 (2011) 78–88.
[16] K. Noh, H. Lim, S. Moon, J.S. Kang, W.J. Lee, D. Lee, Y. Hwang, Mega-dose Vitamin C modulates T cell functions in Balb/c mice only when administered during T cell activation, Immunol. Lett. 98 (2005) 63–72.
[17] E. Klimant, H. Wright, D. Rubin, D. Seely, M. Markman, Intravenous vitamin C in the supportive care of cancer patients: a review and rational approach, Curr. Oncol. 25 (2018) 139–148.
[18] S.J. Padayatty, H. Sun, Y. Wang, H.D. Riordan, S.M. Hewitt, A. Katz, R.A. Wesley, M. Levine, Vitamin C pharmacokinetics: implications for oral and intravenous use, Ann. Intern. Med. 140 (2004) 533.
[19] A. Carr, S. Maggini, Vitamin C and immune function, Nutrients 9 (2017) 1211.
[20] E.T. Creagan, C.G. Moertel, J.R. O'Fallon, A.J. Schutt, M.J. O'Connell, J. Rubin, S. Frytak, Failure of high-dose vitamin C (ascorbic acid) therapy to benefit patients with advanced cancer, N. Engl. J. Med. 301 (1979) 687–690.
[21] M.J. Webber, E.A. Appel, E.W. Meijer, R. Langer, Supramolecular biomaterials, Nat. Mater. 15 (2016) 13–26.
[22] N.M. Sangeetha, U. Maitra, Supramolecular gels: functions and uses, Chem. Soc. Rev. 34 (2005) 821.
[23] F. Wang, D. Xu, H. Su, W. Zhang, X. Sun, M.K. Monroe, R.W. Chakroun, Z. Wang, W. Dai, R. Oh, H. Wang, Q. Fan, F. Wan, H. Cui, Supramolecular prodrug hydrogelator as an immune booster for checkpoint blocker–based immunotherapy, Sci. Adv. 6 (2020), eaaz8985.
[24] Y. Yin, X. Li, H. Ma, J. Zhang, D. Yu, R. Zhao, S. Yu, G. Nie, H. Wang, In situ transforming RNA nanovaccines from polyethylenimine functionalized graphene oxide hydrogel for durable cancer immunotherapy, Nano Lett. 21 (2021) 2224–2231.
[25] J. Zhou, X. Du, B. Xu, Regulating the rate of molecular self-assembly for targeting cancer cells, Angew. Chem. Int. Ed. 55 (2016) 5770–5775.
[26] Z. Luo, Q. Wu, C. Yang, H. Wang, T. He, Y. Wang, Z. Wang, H. Chen, X. Li, C. Gong, Z. Yang, A powerful CD8 + T-cell stimulating D-tetra-peptide hydrogel as a very promising vaccine adjuvant, Adv. Mater. 29 (2017), 1601776.
[27] Y. Chao, L. Xu, C. Liang, L. Feng, J. Xu, Z. Dong, L. Tian, X. Yi, K. Yang, Z. Liu, Combined local immunostimulatory radioisotope therapy and systemic immune checkpoint blockade imparts potent antitumour responses, Nat. Biomed. Eng. 2 (2018) 611–621.
[28] F. Wang, H. Su, D. Xu, W. Dai, W. Zhang, Z. Wang, C.F. Anderson, M. Zheng, R. Oh, F. Wan, H. Cui, Tumour sensitization via the extended intratumoural release of a STING agonist and camptothecin from a self-assembled hydrogel, Nat. Biomed. Eng. 4 (2020) 1090–1101.
[29] F. Rizzo, N.S. Kehr, Recent advances in injectable hydrogels for controlled and local drug delivery, Adv. Healthc. Mater. 10 (2021), 2001341.
[30] M. Chen, Y. Tan, Z. Dong, J. Lu, X. Han, Q. Jin, W. Zhu, J. Shen, L. Cheng, Z. Liu, Q. Chen, Injectable Anti-inflammatory nanofiber hydrogel to achieve systemic immunotherapy post local administration, Nano Lett. 20 (2020) 6763–6773.
[31] L. Zhang, D. Jing, N. Jiang, T. Rojalin, C.M. Baehr, D. Zhang, W. Xiao, Y. Wu, Z. Cong, J.J. Li, Y. Li, L. Wang, K.S. Lam, Transformable peptide nanoparticles arrest HER2 signalling and cause cancer cell death in vivo, Nat. Nanotechnol. 15 (2020) 145–153.
[32] T. Wang, D. Wang, H. Yu, B. Feng, F. Zhou, H. Zhang, L. Zhou, S. Jiao, Y. Li, A cancer vaccine-mediated postoperative immunotherapy for recurrent and metastatic tumors, Nat. Commun. 9 (2018) 1532.
[33] Q. Wu, Z. He, X. Wang, Q. Zhang, Q. Wei, S. Ma, C. Ma, J. Li, Q. Wang, Cascade enzymes within self-assembled hybrid nanogel mimicked neutrophil lysosomes for singlet oxygen elevated cancer therapy, Nat. Commun. 10 (2019) 240.
[34] J. Li, K. Shi, Z.F. Sabet, W. Fu, H. Zhou, S. Xu, T. Liu, M. You, M. Cao, M. Xu, X. Cui, B. Hu, Y. Liu, C. Chen, New power of self-assembling carbonic anhydrase inhibitor: short peptide–constructed nanofibers inspire hypoxic cancer therapy, Sci. Adv. 5 (2019), eaax0937.
[35] X. Du, J. Zhou, B. Xu, Supramolecular hydrogels made of basic biological building blocks, Chem. Asian J. 9 (2014) 1446–1472.
[36] Y. Chao, Q. Chen, Z. Liu, Smart injectable hydrogels for cancer immunotherapy, Adv. Funct. Mater. 30 (2020), 1902785.
[37] H. Ma, C. He, X. Chen, Injectable hydrogels as local depots at tumor sites for antitumor immunotherapy and immune-based combination therapy, Macromol. Biosci. 21 (2021), 2100039.
[38] E.L. Dane, A. Belessiotis-Richards, C. Backlund, J. Wang, K. Hidaka, L.E. Milling, S. Bhagchandani, M.B. Melo, S. Wu, N. Li, N. Donahue, K. Ni, L. Ma, M. Okaniwa, M.M. Stevens, A. Alexander-Katz, D.J. Irvine, STING agonist delivery by tumour-penetrating PEG-lipid nanodiscs primes robust anticancer immunity, Nat. Mater. 21 (2022) 710–720.
[39] S. Li, M. Luo, Z. Wang, Q. Feng, J. Wilhelm, X. Wang, W. Li, J. Wang, A. Cholka, Y. Fu, B.D. Sumer, H. Yu, J. Gao, Prolonged activation of innate immune pathways by a polyvalent STING agonist, Nat. Biomed. Eng. 5 (2021) 455–466.
[40] C. Wang, Y. Guan, M. Lv, R. Zhang, Z. Guo, X. Wei, X. Du, J. Yang, T. Li, Y. Wan, X. Su, X. Huang, Z. Jiang, Manganese increases the sensitivity of the cGAS-STING pathway for double-stranded DNA and is required for the host defense against DNA viruses, Immunity 48 (2018) 675–687, e7.
[41] S. Nandi, H.-J. Altenbach, B. Jakob, K. Lange, R. Ihizane, M.P. Schneider, A novel class of organo- (hydro-) gelators based on ascorbic acid, Org. Lett. 13 (2011) 1980–1983.
[42] Y. Zhao, B. Qu, X. Wu, X. Li, Q. Liu, X. Jin, L. Guo, L. Hai, Y. Wu, Design, synthesis and biological evaluation of brain targeting l-ascorbic acid prodrugs of ibuprofen with "lock-in" function, Eur. J. Med. Chem. 82 (2014) 314–323.
[43] R.W. Chakroun, F. Wang, R. Lin, Y. Wang, H. Su, D. Pompa, H. Cui, Fine-tuning the linear release rate of paclitaxel-bearing supramolecular filament hydrogels through molecular engineering, ACS Nano 13 (2019) 7780–7790.
[44] F. Wang, H. Su, R. Lin, R.W. Chakroun, M.K. Monroe, Z. Wang, M. Porter, H. Cui, Supramolecular tubustecan hydrogel as chemotherapeutic carrier to improve tumor penetration and local treatment efficacy, ACS Nano 14 (2020) 10083–10094.
[45] F. Wang, H. Su, D. Xu, M.K. Monroe, C.F. Anderson, W. Zhang, R. Oh, Z. Wang, X. Sun, H. Wang, F. Wan, H. Cui, Therapeutic supramolecular tubustecan hydrogel combined with checkpoint inhibitor elicits immunity to combat cancer, Biomaterials 279 (2021), 121182.
[46] J.M. Ramanjulu, G.S. Pesiridis, J. Yang, N. Concha, R. Singhaus, S.-Y. Zhang, J.-L. Tran, P. Moore, S. Lehmann, H.C. Eberl, M. Muelbaier, J.L. Schneck, J. Clemens, M. Adam, J. Mehlmann, J. Romano, A. Morales, J. Kang, L. Leister, T.L. Graybill, A. K. Charnley, G. Ye, N. Nevins, K. Behnia, A.I. Wolf, V. Kasparcova, K. Nurse, L. Wang, A.C. Puhl, Y. Li, M. Klein, C.B. Hopson, J. Guss, M. Bantscheff, G. Bergamini, M.A. Reilly, Y. Lian, K.J. Duffy, J. Adams, K.P. Foley, P.J. Gough, R. W. Marquis, J. Smothers, A. Hoos, J. Bertin, Design of amidobenzimidazole STING receptor agonists with systemic activity, Nature 564 (2018) 439–443.
[47] J. Wang, P. Li, Y. Yu, Y. Fu, H. Jiang, M. Lu, Z. Sun, S. Jiang, L. Lu, M.X. Wu, Pulmonary surfactant–biomimetic nanoparticles potentiate heterosubtypic influenza immunity, Science 367 (2020), eaau0810.
[48] I. Mellman, R.M. Steinman, Dendritic cells, Cell 106 (2001) 255–258.
[49] Q. Jin, W. Zhu, J. Zhu, J. Zhu, J. Shen, Z. Liu, Y. Yang, Q. Chen, Nanoparticle-mediated delivery of inhaled immunotherapeutics for treating lung metastasis, Adv. Mater. 33 (2021), 2007557.
[50] X. Yi, H. Zhou, Y. Chao, S. Xiong, J. Zhong, Z. Chai, K. Yang, Z. Liu, Bacteria-triggered tumor-specific thrombosis to enable potent photothermal immunotherapy of cancer, Sci. Adv. 6 (2020) eaba3546.
[51] J. Xu, J. Lv, Q. Zhuang, Z. Yang, Z. Cao, L. Xu, P. Pei, C. Wang, H. Wu, Z. Dong, Y. Chao, C. Wang, K. Yang, R. Peng, Y. Cheng, Z. Liu, A general strategy towards personalized nanovaccines based on fluoropolymers for post-surgical cancer immunotherapy, Nat. Nanotechnol. 15 (2020) 1043–1052.
[52] J. Li, X. Yu, Y. Jiang, S. He, Y. Zhang, Y. Luo, K. Pu, Second near-infrared photothermal semiconducting polymer nanoadjuvant for enhanced cancer immunotherapy, Adv. Mater. 33 (2021), 2003458.